Non-linear optical microscopy as a novel quantitative and label-free imaging modality to improve the assessment of tissue-engineered cartilage

Ashraful Islam[1§], Elisabeth Inge Romijn[2§], Magnus Borstad Lilledahl[2], Inigo Martinez-Zubiaurre[1]

1. Institute of Clinical Medicine, University of Tromsø, Norway

2. Department of Physics, Norwegian University of Science and Technology, Norway

§ Contributed equally

Contact:

ashraful.islam@uit.no

elisabeth.romijn@ntnu.no

magnus.lilledahl@ntnu.no

Corresponding author:

Professor Inigo Martinez-Zubiaurre

Institute of Clinical Medicine, University of Tromsø

9037, Norway

Email: inigo.martinez@uit.no

Phone: (0047)77644686

Running Title: SHG and scoring of engineered cartilage.

Abstract

Objective: Current systems to evaluate outcomes from tissue-engineered cartilage (TEC) are sub-optimal. The main purpose of our study was to demonstrate the use of second harmonic generation (SHG) microscopy as a novel quantitative approach to assess collagen deposition in laboratory made cartilage constructs.

Methods: Scaffold-free cartilage constructs were obtained by condensation of *in vitro* expanded Hoffa's fat pad derived stromal cells (HFPSCs), incubated in the presence or absence of chondrogenic growth factors (GF) during a period of 21 d. Cartilage–like features in constructs were assessed by Alcian blue staining, transmission electron microscopy (TEM), SHG and two-photon excited fluorescence microscopy. A new scoring system, using second harmonic generation microscopy index for collagen density and distribution, was adapted to the existing "Bern score" in order to evaluate *in vitro* TEC.

Results: Spheroids with GF gave a relative high Bern score value due to appropriate cell morphology, cell density, tissue-like features and proteoglycan content, whereas spheroids without GF did not. However, both TEM and SHG revealed striking differences between the collagen framework in the spheroids and native cartilage. Spheroids required a four-fold increase in laser power to visualize the collagen matrix by SHG compared to native cartilage. Additionally, collagen distribution, determined as the area of tissue generating SHG signal, was higher in spheroids with GF than without GF, but lower than in native cartilage.

Conclusion: SHG represents a reliable quantitative approach to assess collagen deposition in laboratory engineered cartilage, and may be applied to improve currently established scoring systems.

Keywords: **Second harmonic generation microscopy, Two-photon excited fluorescence microscopy, Hoffa's fat pad derived stromal cells, Chondrogenesis, Tissue-engineered cartilage.**

Introduction

Tissue-engineered cartilage (TEC) represents an encouraging approach for the treatment of articular cartilage lesions. Efforts to develop laboratory-grown cartilage implants to treat cartilage defects has grown exponentially over the last two decades[1, 2]. The quality of the resulting tissue depends on several critical parameters including the cell source, the presence of chondrogenic growth factors, a suitable and biocompatible cell carrier and other extrinsic factors such as oxygen tension and mechanical loading[3, 4]. TEC must be capable of enduring similar environmental strains as native cartilage. Even though TEC shows promising results in the laboratory their clinical translation is limited[5]. One of the main challenges is to achieve the proper assembly of the immature extracellular matrix (ECM) components into functional structures that mimic those of native tissue. Most literature within the field of laboratory-grown engineered cartilage provides data on ECM gene expressions or proteins but fails to show the degree of tissue maturation through the density and complexity of the collagen network[3, 4, 6].

In order to have a common ground for assessing the quality of engineered neocartilage, a standardised grading system is essential. The Bern score[7] is widely used, and modified versions have been proposed[8, 9]. This score is based on the proteoglycan content from safranin-O (alternatively Alcian blue) staining, together with a morphological assessment of the cells, cell density, and heterogeneity of the constructs (Table 1). However, the Bern score does not take into account the collagen fraction of the ECM. This is a major limitation as the collagen matrix is an essential component to yield the necessary mechanical support for articular cartilage. Common stains used for collagen (such as Masson's trichrome or picrosirius red) often yield very weak staining with engineered cartilage as the collagen fibres are typically insufficiently developed[10]. Immunohistochemical detection of collagen I and II provides only qualitative

information and is not sensitive to fibrils maturation, organization and size. The low collagen content in TEC often make immunolocalization of collagens by traditional immunostaining methods less reproducible and reliable[11, 12]. Furthermore, immunostaining-based approaches are subjected to variations related to different affinities of antibodies from different manufacturers.

A number of label-free approaches exist to image cartilage, comprising some advantages and limitations. Thus, infrared spectroscopy (IRS)[13], micro-computed tomography (micro-CT)[14], magnetic resonance imaging (MRI)[15], and polarised light microscopy (PLM)[16] have also been used to measure collagen content in native cartilage, mostly to analyse repaired tissue or to assess osteoarthritis development. However, IRS and micro-CT are complicated and often associated with lack of molecular specificity, while MRI resolution is suboptimal to visualize tissue constructs like other histological techniques and it could be more challenging with TEC. In addition, PLM is also concerned with lack of molecular specificity compared to electron-microscopic stereology[16]. Notably, transmission electron microscopy (TEM) requires rigorous sample preparation[17], and at high magnification it gives information on fibrils composition and organization, but only permits visualization of tissue regions at a nanoscale, which complicates the generalization of the assessments. .

Second harmonic generation (SHG) microscopy is a technique which can be used for quantitative, label-free imaging of collagen in cartilage and is highly sensitive to the ordering of the collagen molecules at the fibril level. It, therefore, represents a promising alternative to traditional staining techniques and could be used in an extension of the Bern score to also evaluate the collagen fraction of the ECM.

SHG is a nonlinear optical effect that is exhibited by non-centrosymmetric molecules. In this process, two photons of a certain wavelength (typically around 800 nm) are converted into a single photon with half the wavelength. The process is strongly enhanced if multiple molecules are aligned within the focal volume. Collagen fibrils are non-centrosymmetric and consist of aligned and ordered collagen molecules and thus yield a strong SHG signal without any labeling. Three-dimensional (3D) imaging is possible due to the intrinsic confocality of multiphoton microscopy. Unlike traditional techniques, no extensive sample preparation is necessary due to the endogenous nature of the signal. This allows for real-time, and non-destructive imaging of the temporal development of engineered tissues[18, 19]. Example applications are assessment of early stage osteoarthritic human cartilage[20], *in vivo* cartilage repair in a rabbit model[21, 22], and scaffold-based TEC[19, 23, 24]. The technique has also been applied successfully to label-free imaging of the ECM in numerous different tissue types such as blood vessels, cornea, liver, bone, skin, and tumour[25-27].

The SHG signal provides a measure of the size, amount, and structure of collagen fibrils[23, 24]. The signal scales quadratically with the molecular concentration and the direction of the emitted SHG signal is dependent on the size of the fibrils[28, 29]. Larger fibrils and thicker fibres lead to an increase in forward second harmonic generation (FSHG) but do not affect the backward second harmonic generation (BSHG) [30, 31]. In addition, the SHG intensity depends on the angle between the laser polarization and the collagen fibril. Polarization-resolved SHG has been reported to be able to distinguish between different collagen types[32, 33]. Since no commercial systems for nonlinear optical microscopy are currently delivered with polarization optics control, we have opted to base our proposed scoring system on SHG signals without polarization-resolved measurement. Such a system has a larger potential for wide-spread adoption.

The aim of this paper is to introduce SHG as a method to assess the quality of *in vitro* TEC and to define a new index based on this signal that can be used as an extension to the existing Bern score, thus providing a more accurate assessment of TEC. We denote the new scoring parameter as second harmonic generation index (SHGI). The unique characteristics of SHG microscopy make it a valuable label-free technique to measure sub-resolution structural information of the collagen matrix with high sensitivity and specificity.

Materials and Methods

HUMAN MATERIALS

Human tissue specimens were collected at the University Hospital of Northern Norway. Fresh Hoffa's fat pad and macroscopically good-looking cartilage samples were collected from knee joints of three patients aged between 45 and 60 years scheduled for total knee replacement surgery. All patients provided written informed consent. The project was approved by the Regional Ethical Committee of Northern Norway (REK Nord 2014/920).

ISOLATION AND CULTURE OF HOFFA'S FAT PAD DERIVED STROMAL CELLS

Hoffa's fat pad derived stromal cells (HFPSCs) were isolated using a mixed enzymatic-explant method as previously described[3]. Briefly, Hoffa's fat pad specimens were washed three times with sterile Dulbecco's phosphate buffered saline (DPBS; Cat. no. D8537; Sigma-Aldrich). The fat tissues were carefully separated from the synovial membrane and minced into small pieces for enzymatic digestion in collagenase XI solution (Cat. no. C9407; Sigma-Aldrich) at a final

concentration of 1.25 mg/mL for 1.5 h on a shaker at 37 °C. Partially digested tissues were collected from the bottom fraction after centrifugation for 10 min at 800g and subsequently re-suspended in a growing medium containing high glucose Dulbecco's Modified Eagle Medium (DMEM; Cat. no. D5796; Sigma-Aldrich) supplemented with L-ascorbic acid (62 mg/L) (Cat. no.103033E; BDH Laboratory), penicillin and streptomycin (1 %) (P/S; Cat. no. P4333; Sigma-Aldrich) and 20 % foetal bovine serum (FBS; Cat. no. S0115; Biochrom) and incubated at 37 °C in a humidified atmosphere containing 5 % CO_2. After initial cell attachment for 24 h, the primary culture of HFPSCs were expanded in 10 % FBS supplemented conditioning medium and basic fibroblast growth factor (25 ng/mL) (bFGF; Cat. no. 100-18C; Peprotech) was added to the culture medium upon reaching 50 % confluence.

CHONDROGENESIS OF HFPSCs AND 3D CULTURE

Chondrogenesis of HFPSCs was achieved using the pellet culture system as previously described[3]. Briefly, HFPSCs at passage three were harvested and transferred to each well of a poly-HEMA (Cat. no. P3932; Sigma-Aldrich) coated conical-bottom 96 well culture plate (Cat. no. 249935; Thermo Scientific) at a density of 5 x 10^4 cells in 150 µl, followed by centrifugation of plates for 10 min at 1100g. Chondrogenesis was induced by incubation in the serum-free chondrogenic medium for 21 d in low oxygen (3 % O_2). The chondrogenic medium contained high glucose DMEM, L-ascorbic acid (62 mg/L), P/S (1 %), dexamethasone (1 µg/mL) (Cat. no. PZN-3103491; Galenpharma), Insulin-transferrin-selenium supplement (ITS) (1:1000) (Cat. no. 354351; BD Biosciences), transforming growth factor β3 (10 ng/mL) (TGF-β3; Cat. no. 100-36E; Peprotech) and bone morphogenic protein 2 (100 ng/mL) (BMP-2; Cat. no. 120-02C; Peprotech). In this study, the growth factors-free medium was identical to the chondrogenic medium but did not include TGF-β3 and BMP-2.

PREPARATION OF TISSUE SECTIONS FOR NON-LINEAR MICROSCOPY

Native cartilage (*n* = 3), spheroids with growth factors (GF) (n = 1, diameter ≈ 1.4 mm) and spheroids without GF (n = 1, diameter ≈ 0.6 mm) were harvested, washed in ice-cold DPBS and fixed in 4 % formalin overnight. Fixed materials were embedded in agarose blocks (1 %) and transferred further into paraffin blocks. Paraffin-embedded sections (4 µm) were heated at 60 °C for 1 h prior to de-waxing and a series of xylene and ethanol washes followed by mounting a cover slip with Histokit (Cat. no. 1025/500; Glaswarenfabrik Karl Hect).

STAINING OF EXTRACELLULAR MATRIX PROTEOGLYCANS BY ALCIAN BLUE

Metachromatic staining was done in this study as previously described[3]. Briefly, Alcian blue solution (Cat. no. A5268; Sigma-Aldrich) was used to stain 4 µm sections for 30 min. Nuclear fast red solution (Cat. no. N3020; Sigma-Aldrich) was used to counterstain the sections for 5 min. Finally, the sections were dehydrated in a series of ethanol and xylene wash followed by mounting a cover slip with Histokit. Images were taken using bright field light microscopy (Leica DMI6000B). Stained sections were scored blindly by three different observers.

TRANSMISSION ELECTRON MICROSCOPY

Ultra-structural analysis was studied using TEM as previously described[3]. Briefly, after harvesting, tissues were fixed overnight in McDowell's fixative[34] and prepared according to our standard laboratory procedure. Sections were cut on a Leica Ultracut S (Vienna, Austria).

TEM images were taken with a JEOL 1010 (Tokyo, Japan) electron microscope and a Morada camera system (Olympus Soft Imaging Systems, Germany).

SECOND HARMONIC GENERATION MICROSCOPY

Images were collected on a confocal microscope (TCS SP8, Leica) equipped with a Ti:Sapphire laser (Chameleon Vision-S, Coherent) tuned to an excitation wavelength of 890 nm. For imaging, a 25x, 0.95 NA water immersion objective and 0.9 NA collector lens were used. The two-photon fluorescence (TPEF) was acquired simultaneously with SHG. In the epi-direction, two HyD detectors combined with a 500-550 nm and 435-455 nm bandpass filter were used to record TPEF and backward (B) scattered SHG, respectively. Forwards (F) scattered SHG was acquired in the transmitted direction using a 435-455 nm band-pass filter in front of a PMT. All images were 1024x1024 pixels and covered an area of 232x232 µm.

Native cartilage was used as a reference to adjust microscope settings, including illumination intensity. To ascertain the reproducibility of the method, native cartilage from three different donors were used. For spheroids with and without growth factors, we have used cells from only one donor since inter-donor comparisons was not the aim of this study and it would not have added meaningful information to the reproducibility of the approach. All images from cartilage were taken from the middle zone to avoid the intra-sample variations due to inherent tissue zonation. Identical settings, except illumination intensity, was used to image spheroids. The laser power used to image native cartilage was about 20mW. Due to a sparser collagen network in the spheroids, the laser power was increased until the BSHG intensity was approximately equal to that generated by native cartilage, i.e. the intensity distributions peaked at the same gray level (50 in a scale of 0 to 255) (Fig 5 d). If a similar intensity was not achieved at a relative

increase in laser power (r_P) of four times the original, then the sample was imaged at this limit. For visual presentation, the square root of the SHG and TPEF intensity are displayed in the images. For analysis, the original images were used. All samples were imaged with the same microscopic settings. To test the reproducibility of reference samples, five areas in each donor were imaged and the laser power was adjusted until the BSHG intensity was equal. The 15 separate reference settings were used to image and analyse a single area in both types of TEC.

Larger fibrils and thicker fibres lead to an increase in FSHG but do not affect the BSHG[30, 31]. In order to compare FSHG and BSHG, the ratio between the FSHG and BSHG (F/B-ratio) was calculated for every pixel within a region of interest for each sample. Image processing and analysis was performed in Matlab (Mathworks) and ImageJ.

SECOND HARMONIC GENERATION INDEX

The SHGI was generated from two individual parameters: the necessary relative increase in laser power (r_P) and the area (A) covered by the collagen matrix (Table 2).

PARAMETER 1: COLLAGEN DENSITY

The density of the collagen network is related to the laser power required to image the sample. To create a relatively objective grading, the laser power used to image the spheroids is increased until the SHG signal is of similar intensity as that in native cartilage, or until the laser power is quadrupled compared to the one used to image native cartilage. An increase in relative laser power (r_P) indicates a less developed collagen network in the tissue-engineered sample.

PARAMETER 2: COLLAGEN DISTRIBUTION

After imaging, the collagen distribution in the image was determined by segmenting the image to determine the area containing significant collagen content. To determine a good threshold, a few regions containing solely ECM (and no lacunae) were selected in the BSHG images of native cartilage. An intensity histogram of the combined areas was made, and a Gaussian curve was fitted to the lower half of the distribution. The threshold was defined to be the average minus three standard deviations ($\mu - 3\sigma$). This is an appropriate threshold to distinguish between the collagen network and background because the difference in SHG signal between native and engineered cartilage has been compensated for by adjusting the laser power. The percentage of area covered by collagen, (A) is used to grade the collagen distribution.

Results

CHONDROGENESIS OF HFPSCs IN 3D CULTURES AND HISTOMORPHOLOGY

TEC was achieved by applying the pellet culture system to HFPSC previously expanded in monolayer cultures. To test the sensitivity of the SHGI, we made HFPSC spheroids incubated in the presence or absence of growth factors. Metachromatic staining of spheroids with GF demonstrated good cartilage-like morphology with abundant proteoglycans in the ECM, and cells with round shaped morphology (Fig. 1 c and d). In contrast, spheroids without GF demonstrated low intensity and areal coverage of Alcian blue stain, high density of cells with irregular morphology, and a lack of lacunae-like structures (Fig. 1 e and f). Histological scoring of samples using the standard Bern score is presented in (Fig. 2).

ULTRASTRUCTURAL ANALYSIS OF 3D SPHEROIDS

TEM was used for visualization of the ECM and cellular characteristics in spheroids and cartilage. TEM images showed a clear difference in collagen structures and orientation when comparing native cartilage and spheroids. Spheroids with GF showed relatively abundant ECM with identifiable and randomly oriented collagen fibrils (Fig. 3 b, e and h). In contrast, collagen fibrils were densely packed and arranged in regular patterns in native cartilage (Fig. 3 a, d and g). In spheroids with GF, the presence of collagen fibrils was prominent around the pericellular regions and gradually replaced with smaller collagen fibrils in the interterritorial space (Fig. 3 b, e and h). Spheroids without GF had cells that were packed more densely with irregular shapes and less ECM production (Fig. 3 c, f and i).

ANALYSIS BY SHG

Native cartilage generated a strong SHG signal from the dense and homogenous ECM with a sparse distribution of lacunae (Fig. 4). The FSHG signal showed enhanced contrast as compared to the BSHG which was more homogeneous. The different donors generated similar SHG and TPEF intensities except one donor that displayed a strong homogeneous TPEF background from the matrix (Fig. 4 a). At the same laser power as used for native cartilage, the spheroids generated negligible SHG signal (r_p=1, Fig. 4). A four-fold relative increase (r_P) in laser power gave images that showed the ECM clearly (r_p=4, Fig. 4). However, increasing the laser power above that threshold resulted in photo-damage of the samples. Spheroids with GF showed cartilage-like appearance with clear lacunae-like structures and ECM production (Fig. 4 b, e and h). However, the collagen deposits were more irregular and uneven when compared to

native cartilage. The spheroids without GF generated a weaker SHG signal even at maximum laser power (Fig. 4 c, f and i).

At a four-fold increase in laser power, there was still a reasonable area that contained SHG signal above the threshold, defined as collagen matrix in the spheroids with GF (*A*=37%, Fig. 5 b and e). In contrast, spheroids without GF displayed a minimal area that contained an SHG signal above threshold (*A*=9%, Fig. 5 c and f). Using five different areas in each donor as a reference confirmed that there was a clear trend in amount of collagen matrix for each experimental sample (Fig. 5 g), which is also distinguishable when using a single donor (Fig. 4 h), despite inter and intra variation caused by the change of a reference sample. Results from SHGI along with standard Bern score for samples are presented in Fig. 2. The F/B-ratio was similar for all samples, despite their difference in overall SHG intensity (Fig. 6).

Discussion

The main objective of this study was to assess collagen deposits in TEC by means of SHG microscopy and to include an index based on this measurement in existing Bern score for assessment of TEC. The application of SHG microscopy to analyse cartilage is still in its infancy, but has recently been used to analyse TEC[19, 21, 23, 24, 35].

Due to a sparser collagen matrix in spheroids compared to native cartilage, a noticeable difference was observed in the SHG intensity (Fig. 4 d-i). Weak SHG signals in TEC have also been reported in previous studies[19, 23]. However, at a four-fold increase in power (r_p), the collagen matrix in spheroids became clearly visible (right column, Fig. 4 d and e). Ample differences in the collagen network were confirmed by TEM examination of the samples, which

revealed a lack of collagen *fibres* and presence of only sparsely distributed *fibrils* in spheroids with GF compared to native cartilage (Fig. 3 a, b, d, e, g and h). Spheroids without GF displayed a strong TPEF signal while almost no SHG was detectable (Fig. 4). This is in agreement with the results from histology and TEM (Fig. 1 e and f, and 3 c, f and i), which demonstrated a very high density of cells, with a sparsely formed ECM.

Based on the original scoring system spheroids with and without GF resulted in Bern scores of 8 and 1 in a scale of 9, (Fig. 2). However, with the SHGI extended Bern score, spheroids with and without GF resulted in scores of 9 and 1 in a scale of 12, which provides a more precise assessment of the constructs when compared to native cartilage (Fig. 2). The inclusion of the SHGI into the existing scoring categories revealed a more complete description of the ECM constructs that balanced the high Bern score obtained by scoring only proteoglycans staining. Variations within reference samples could be a source of uncertainty in the proposed SHGI (Fig. 5 g and h). The relative laser power (r_p) in our low collagen content TEC was constant, independently of the reference sample used. However, the area giving sufficient collagen signal (A) is more sensitive than if a clear peak could be achieved in the intensity histogram (Fig. 5 e and f). As a counter measure both the SHGI subcategory based on relative laser power (r_p) and collagen area (A) have a quite crude division, which limits the effect on the overall SHGI grade.

The F/B ratio can be used as an additional tool to assess collagen fibres in TEC. However, the F/B ratio is affected by multiple properties of collagen fibres and fibrils, their diameter, uniformity of fibrils within the fibre, and density[30, 36]. Thicker fibres/fibrils and the bundling of collagen fibrils into fibres lead to an increase in FSHG but hardly affects the BSHG, thereby giving an increase in the F/B-ratio. However, previous studies have shown by numerical simulation that the F/B ratio is unchanged by variation of filling ratio, and collagen fibrils within

the focal volume, even though densely packed collagen fibrils give an increase in overall signal[28, 37]. In our study, we observed no difference in F/B ratio when comparing the collagen network of the spheroids with native cartilage (Fig. 6). This confirms the interpretation that the lower SHG signal from the engineered cartilaginous tissue was due to a decrease in collagen density, rather than smaller fibrils. The brighter fibrillar structure visible in the pericellular region of the spheroids with GF demonstrated no difference in F/B-ratio compared to the surrounding matrix, which agrees with the interpretation that the increase in intensity was caused by densely packed fibrils in this area.

Previously published studies have not used SHG in a scoring system and referenced the assessments with native cartilage. In line with our study, both Olderoy *et al.*[23] and Filova *et al.*[38] reported relatively evenly distributed SHG signal from TEC generated under certain conditions. However, the intensity of the signal was not compared to that of native cartilage, and therefore it is difficult to determine the density of the collagen matrix from solely evaluating the SHG signal. Maehara *et al.*[19] created TEC using collagen type I gel scaffolds. In these samples, the produced collagen II generated such a weak SHG signal compared to the thick collagen type I fibers in the scaffold that the generated matrix was observed as dark areas in the bright scaffold. The signal generated by the collagen in the scaffold would interfere with the (r_p) adjustment. It will, therefore, be more troublesome to apply the SHGI to TEC that have used collagen-based scaffolds. It is acknowledged that the use of mechanical stimulation, such as compressive, and shear forces, promotes collagen production and improves collagen orientation during *in vitro* chondrogenesis[39, 40]. Hence, we presume that SHGI could be improved in TEC if mechanical stimulation is applied during *in vitro* chondrogenesis, or if constructs are matured by transient *in vivo* incubations.

The current study is focused on assessing the robustness of the experimental technique with a special emphasis on the variability of the reference samples. To validate the technique with respect to biological variability of the TEC, a larger data set and quantitative comparison with a gold standard for collagen content, e.g. TEM, is needed. Another limitation is that without polarization-resolved SHG microscopy, it is not possible to discern between different collagen types. This is a relevant issue since identification of different collagens permits the differentiation between different cartilaginous tissues. In most instances, TEC produce both collagen type I and type II. Polarization-resolved SHG could provide additional information on the proportion of collagen type I and II in the constructs[32, 33, 41]. However, as mentioned in the introduction, no commercial *nonlinear microscopes* are currently delivered with polarization optics control and its reproduction would require substantial technical expertise. In addition, most analytical models of polarization-resolved SHG images requires ordered fibrils which lie in the imaging plane and might not be possible to use on the disordered collagen structure of TEC. Under such circumstances, specific immunodetection of collagens would provide qualitative information on the collagen types present in the ECM. Future work will emphasize the use of polarization techniques along with the newly proposed SHGI in order to evaluate the applicability to TEC.

Conclusion

In this study, we introduce SHG as a new, quantitative, and label-free approach to analyse the collagenous fraction in TEC and propose a new scoring system for based on the existing Bern score with an additional index representing quantitative assessments of collagen density and distribution by SHG. Introducing a new scoring that considers the collagen fraction in the matrix improves markedly the assessment of engineered cartilage.

Acknowledgements

This work is supported by University of Tromsø and Norwegian University of Science and Technology. Special thanks to Drs. Gunnar Knutsen and Geir Tore Abrahamsen, University Hospital of North Norway (UNN), for providing cartilage and Hoffa's fat pad biopsies. The authors sincerely thank Kirsti Rønne and Augusta Aspar for preparing sections for imaging.

Contributions

AI and EIR wrote the first draft of the manuscript. AI primarily prepared the final draft of the manuscript and conducted the laboratory work. EIR analyzed the SHG images. MBL and IMZ planned the study, edited and approved the final manuscript.

Ethical statement

The Regional Ethical Committee of Northern Norway has approved the study.

Competing interests

The authors declare no competing interests.

References

1. Filardo G, Vannini F, Marcacci M, Andriolo L, Ferruzzi A, Giannini S, et al. Matrix-assisted autologous chondrocyte transplantation for cartilage regeneration in osteoarthritic knees: results and failures at midterm follow-up. Am J Sports Med 2013; 41: 95-100.
2. Brittberg M. Autologous chondrocyte implantation--technique and long-term follow-up. Injury 2008; 39 Suppl 1: S40-49.
3. Islam A, Hansen AK, Mennan C, Martinez-Zubiaurre I. Mesenchymal stromal cells from human umbilical cords display poor chondrogenic potential in scaffold-free three dimensional cultures. Eur Cell Mater 2016; 31: 407-424.
4. Ding DC, Wu KC, Chou HL, Hung WT, Liu HW, Chu TY. Human Infrapatellar Fat Pad-Derived Stromal Cells Have More Potent Differentiation Capacity Than Other Mesenchymal Cells and Can Be Enhanced by Hyaluronan. Cell Transplant 2015; 24: 1221-1232.
5. Knutsen G, Drogset JO, Engebretsen L, Grontvedt T, Isaksen V, Ludvigsen TC, et al. A randomized trial comparing autologous chondrocyte implantation with microfracture. Findings at five years. J Bone Joint Surg Am 2007; 89: 2105-2112.
6. Bailey MM, Wang L, Bode CJ, Mitchell KE, Detamore MS. A comparison of human umbilical cord matrix stem cells and temporomandibular joint condylar chondrocytes for tissue engineering temporomandibular joint condylar cartilage. Tissue Eng 2007; 13: 2003-2010.
7. Grogan SP, Barbero A, Winkelmann V, Rieser F, Fitzsimmons JS, O'Driscoll S, et al. Visual histological grading system for the evaluation of in vitro-generated neocartilage. Tissue Eng 2006; 12: 2141-2149.

8. Im GI, Shin YW, Lee KB. Do adipose tissue-derived mesenchymal stem cells have the same osteogenic and chondrogenic potential as bone marrow-derived cells? Osteoarthritis Cartilage 2005; 13: 845-853.

9. Zhongcheng G, Hui X, Xing L, Lili W, Jian L, Yang W, et al. Use of synovium-derived stromal cells and chitosan/collagen type I scaffolds for cartilage tissue engineering. Biomedical Materials 2010; 5: 055005.

10. Puchtler H, Meloan SN, Waldrop FS. Are picro-dye reactions for collagens quantitative? Chemical and histochemical considerations. Histochemistry 1988; 88: 243-256.

11. Freed LE, Hollander AP, Martin I, Barry JR, Langer R, Vunjak-Novakovic G. Chondrogenesis in a cell-polymer-bioreactor system. Exp Cell Res 1998; 240: 58-65.

12. Kafienah W, Jakob M, Demarteau O, Frazer A, Barker MD, Martin I, et al. Three-dimensional tissue engineering of hyaline cartilage: comparison of adult nasal and articular chondrocytes. Tissue Eng 2002; 8: 817-826.

13. Rieppo L, Saarakkala S, Jurvelin JS, Rieppo J. Optimal variable selection for Fourier transform infrared spectroscopic analysis of articular cartilage composition. Journal of Biomedical Optics 2014; 19: 027003-027003.

14. Nieminen HJ, Ylitalo T, Karhula S, Suuronen JP, Kauppinen S, Serimaa R, et al. Determining collagen distribution in articular cartilage using contrast-enhanced micro-computed tomography. Osteoarthritis Cartilage 2015; 23: 1613-1621.

15. Ross KA, Williams RM, Schnabel LV, Mohammed HO, Potter HG, Bradica G, et al. Comparison of Three Methods to Quantify Repair Cartilage Collagen Orientation. Cartilage 2013; 4: 111-120.

16. Langsjo TK, Rieppo J, Pelttari A, Oksala N, Kovanen V, Helminen HJ. Collagenase-induced changes in articular cartilage as detected by electron-microscopic stereology,

quantitative polarized light microscopy and biochemical assays. Cells Tissues Organs 2002; 172: 265-275.

17. Meknas K, Johansen O, Steigen SE, Olsen R, Jorgensen L, Kartus J. Could tendinosis be involved in osteoarthritis? Scand J Med Sci Sports 2012; 22: 627-634.

18. Campagnola PJ, Millard AC, Terasaki M, Hoppe PE, Malone CJ, Mohler WA. Three-dimensional high-resolution second-harmonic generation imaging of endogenous structural proteins in biological tissues. Biophys J 2002; 82: 493-508.

19. Maehara R, Fukushima S, Kino-Oka M, Araki T. Non-invasive detection of matrix-producing chondrocytes in tissue-engineered cartilage by second-harmonic-generation microscopy. Journal of Biomechanical Science and Engineering 2014; 9: JBSE0007-JBSE0007.

20. Kumar R, Gronhaug KM, Davies CL, Drogset JO, Lilledahl MB. Nonlinear optical microscopy of early stage (ICRS Grade-I) osteoarthritic human cartilage. Biomed Opt Express 2015; 6: 1895-1903.

21. Bordeaux-Rego P, Baratti MO, Duarte ASS, Ribeiro TB, Andreoli-Risso MF, Vidal B, et al. Use of the second harmonic generation microscopy to evaluate chondrogenic differentiation of mesenchymal stem cells for cartilage repair. vol. 82262012:82263N-82263N-82269.

22. Zhu XQ, Xu YH, Liao CX, Liu WG, Cheng KK, Chen JX. Differentiating the extent of cartilage repair in rabbit ears using nonlinear optical microscopy. Journal of Microscopy 2015; 260: 219-226.

23. Olderoy MO, Lilledahl MB, Beckwith MS, Melvik JE, Reinholt F, Sikorski P, et al. Biochemical and structural characterization of neocartilage formed by mesenchymal stem cells in alginate hydrogels. PLoS One 2014; 9: e91662.

24. Chen WL, Huang CH, Chiou LL, Chen TH, Huang YY, Jiang CC, et al. Multiphoton imaging and quantitative analysis of collagen production by chondrogenic human mesenchymal stem cells cultured in chitosan scaffold. Tissue Eng Part C Methods 2010; 16: 913-920.

25. Sun T-L, Liu Y, Sung M-C, Chen H-C, Yang C-H, Hovhannisyan V, et al. Ex vivo imaging and quantification of liver fibrosis using second-harmonic generation microscopy. Journal of Biomedical Optics 2010; 15: 036002-036002-036006.

26. Tilbury K, Campagnola PJ. Applications of second-harmonic generation imaging microscopy in ovarian and breast cancer. Perspect Medicin Chem 2015; 7: 21-32.

27. Zoumi A, Lu X, Kassab GS, Tromberg BJ. Imaging coronary artery microstructure using second-harmonic and two-photon fluorescence microscopy. Biophys J 2004; 87: 2778-2786.

28. Houle M-A, Couture C-A, Bancelin S, Van der Kolk J, Auger E, Brown C, et al. Analysis of forward and backward Second Harmonic Generation images to probe the nanoscale structure of collagen within bone and cartilage. Journal of Biophotonics 2015; 8: 993-1001.

29. Williams RM, Zipfel WR, Webb WW. Interpreting Second-Harmonic Generation Images of Collagen I Fibrils. Biophysical Journal; 88: 1377-1386.

30. Lacomb R, Nadiarnykh O, Townsend SS, Campagnola PJ. Phase Matching considerations in Second Harmonic Generation from tissues: Effects on emission directionality, conversion efficiency and observed morphology. Opt Commun 2008; 281: 1823-1832.

31. Williams RM, Zipfel WR, Webb WW. Interpreting second-harmonic generation images of collagen I fibrils. Biophys J 2005; 88: 1377-1386.

32. Su P-J, Chen W-L, Chen Y-F, Dong C-Y. Determination of Collagen Nanostructure from Second-Order Susceptibility Tensor Analysis. Biophysical Journal 2011; 100: 2053-2062.

33. Kumar R, Grønhaug KM, Romijn EI, Finnøy A, Davies CL, Drogset JO, et al. Polarization second harmonic generation microscopy provides quantitative enhanced molecular specificity for tissue diagnostics. Journal of Biophotonics 2015; 8: 730-739.

34. McDowell EM, Trump BF. Histologic fixatives suitable for diagnostic light and electron microscopy. Arch Pathol Lab Med 1976; 100: 405-414.

35. Chen T, Hilton MJ, Brown EB, Zuscik MJ, Awad HA. Engineering superficial zone features in tissue engineered cartilage. Biotechnol Bioeng 2013; 110: 1476-1486.

36. Chaudhary R, Campbell KR, Tilbury KB, Vanderby R, Jr., Block WF, Kijowski R, et al. Articular cartilage zonal differentiation via 3D Second-Harmonic Generation imaging microscopy. Connect Tissue Res 2015; 56: 76-86.

37. Brown CP, Houle M-A, Popov K, Nicklaus M, Couture C-A, Laliberté M, et al. Imaging and modeling collagen architecture from the nano to micro scale. Biomedical Optics Express 2014; 5: 233-243.

38. Filova E, Burdikova Z, Rampichova M, Bianchini P, Capek M, Kostakova E, et al. Analysis and three-dimensional visualization of collagen in artificial scaffolds using nonlinear microscopy techniques. J Biomed Opt 2010; 15: 066011.

39. Waldman SD, Couto DC, Grynpas MD, Pilliar RM, Kandel RA. Multi-axial mechanical stimulation of tissue engineered cartilage: review. Eur Cell Mater 2007; 13: 66-73; discussion 73-64.

40. Guo T, Yu L, Lim CG, Goodley AS, Xiao X, Placone JK, et al. Effect of Dynamic Culture and Periodic Compression on Human Mesenchymal Stem Cell Proliferation and Chondrogenesis. Ann Biomed Eng 2016; 44: 2103-2113.

41. Su PJ, Chen WL, Li TH, Chou CK, Chen TH, Ho YY, et al. The discrimination of type I and type II collagen and the label-free imaging of engineered cartilage tissue. Biomaterials 2010; 31: 9415-9421.

Table 1. Proposed scoring categories for evaluation of chondrogenesis of tissue-engineered cartilage. Original Bern score: Category 1-3 and SHGI: Category 4

Scoring Categories	**Score**
1. **Uniformity and intensity of Alcian blue stain**	
No stain	0
Weak stain of matrix	1
Moderate stain	2
Strong stain of matrix	3
2. **Matrix formation based on proteoglycan staining**	
No matrix formation	0
Little matrix formation with high cell density	1
Moderate matrix formation with relatively low cell density	2
High matrix formation with low cell density	3
3. **Cell morphology**	
Highly condensed and elongated cells	0
Less condensed and elongated/rounded cells	1
Mixed elongated/rounded cells with lacunae	2
Rounded Cells with Lacunae/cartilage morphology	3
4. **Second harmonic generation microscopy index (SHGI)**	
Combined score 0	0
Combined score 1-2	1
Combined score 3-4	2
Combined score 4-6	3
Overall Score Range	**0-12**

Table 2. Two individual parameters used to generate SHGI.

SHGI	**Score**
1. **Laser power required (compared to native cartilage), (r_p)**	
>4 times	0
>3 to 4 times	1
>2 to 3 times	2
1 to 2 times	3
2. **Area covered by collagen (*A*)**	
<25%	0
25-50%	1
50-75%	2
>75-100%	3
SHGI Range	**0-6**

Figure 1. Light microscopy images at different experimental stages. Light microscopy images of thin sections (4 µm), stained for proteoglycans with Alcian blue, and the nuclei counterstained with Sirius red, from (a and b) cartilage, (c and d) HFPSCs spheroid (+GF) and (e and f) HFPSCs spheroid (-GF) at low and high magnification with scale bar 200 µm and 5 µm, respectively.

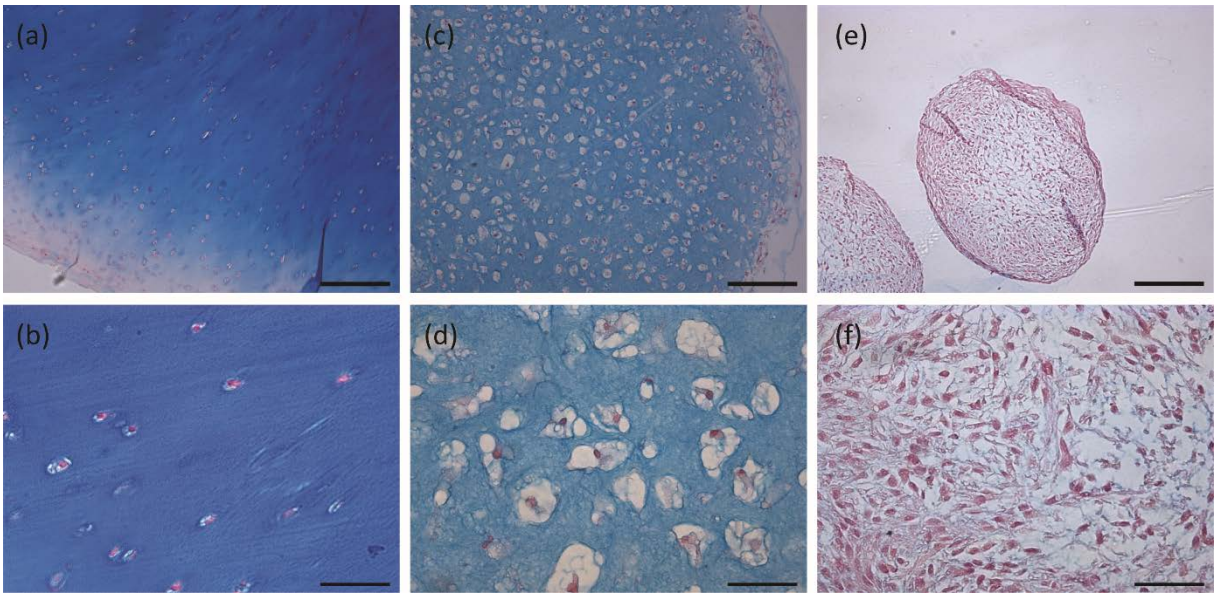

Figure 2. Visual histological grading of samples using standard Bern score and Bern score + SHGI.

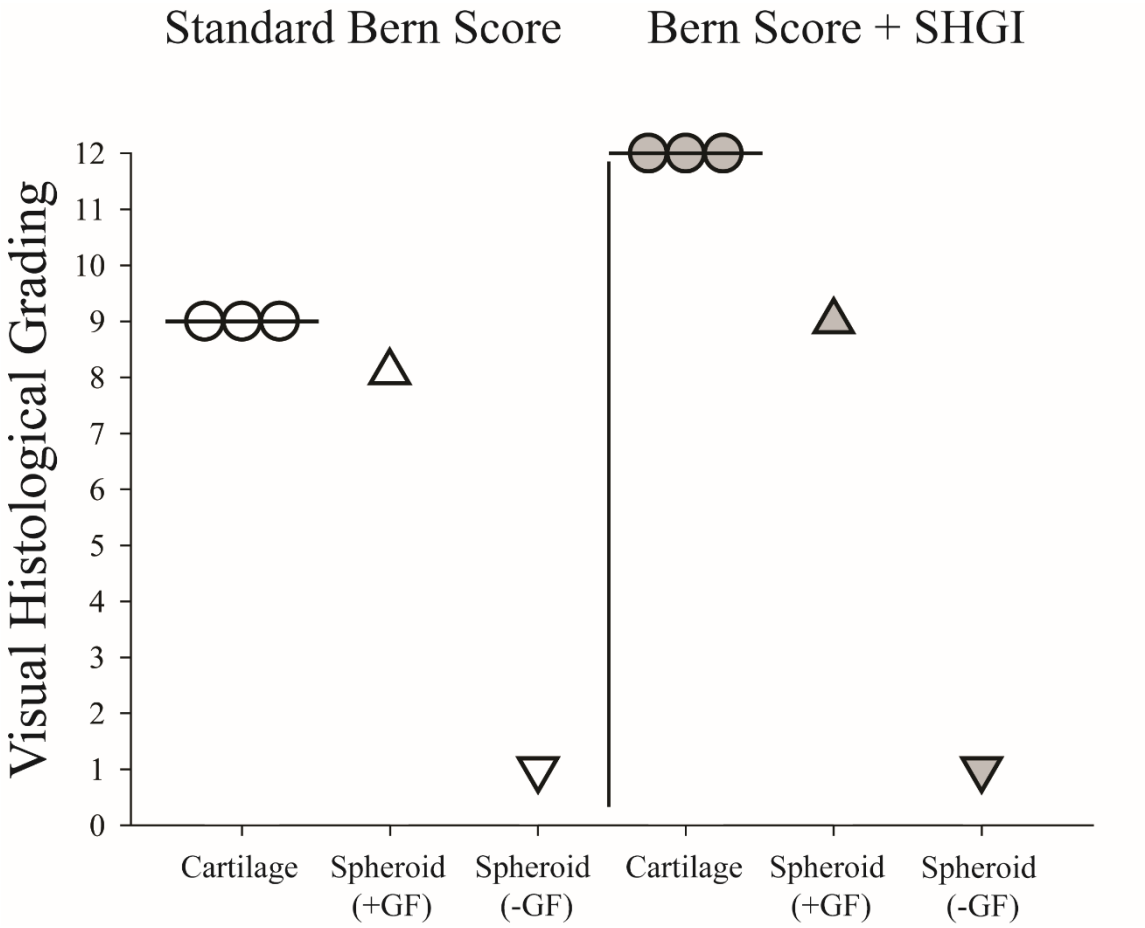

Figure 3. Transmission electron micrograph (TEM) images of of ultra-thin sections of 3D spheroids and cartilage. (a) Cartilage, (b) HFPSCs spheroid (+GF) and (c) HFPSCs spheroid (-GF) at 5000x magnification and scale bar: 10 µm. ECM of (d and g) cartilage, (e and h) HFPSCs spheroid (+GF) and (f and i) HFPSCs spheroid (-GF) at 8000x and 40000x magnification with 5 µm and 1 µm scale bar, respectively. Symbols: * = Cell, (ECM) = Extracellular matrix, (→) = Collagen fibril and (bold ↑) = Collagen fibres.

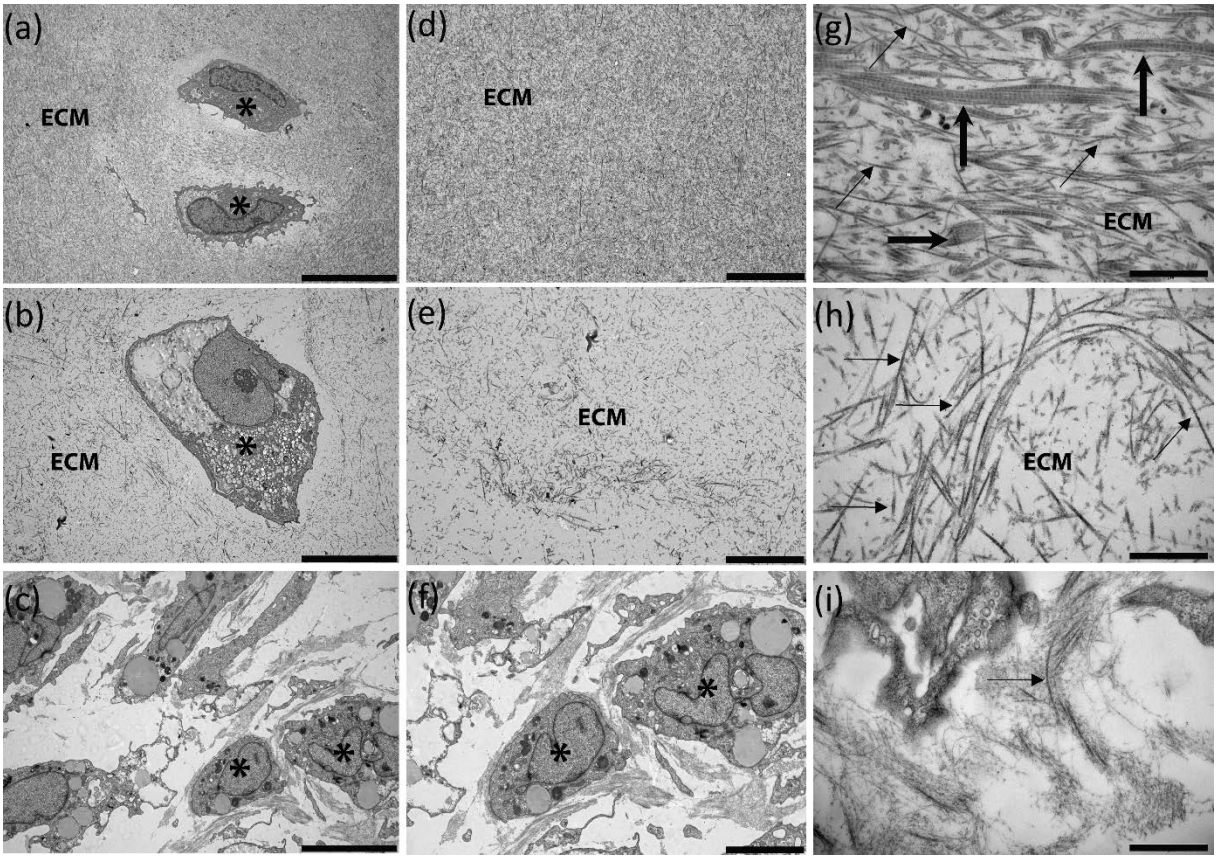

Figure 4. Second harmonic generation microscopy (SHGM) images of thin sections of 3D spheroids and cartilage. (a) Cartilage from three different donors, (b) HFPSCs spheroid (+GF) and (c) HFPSCs spheroid (-GF) imaged by TPEF, BSHG and FSHG to visualize the difference in generated signal. All donors were imaged with the same microscope settings. The tissue-engineered cartilage images were divided into four sections based on a relative increase in laser power (r_P) of one, two, three and four times (left to right) compared to native cartilage. The rest of the microscope settings remained same between imaging. Scale bar: 50 µm.

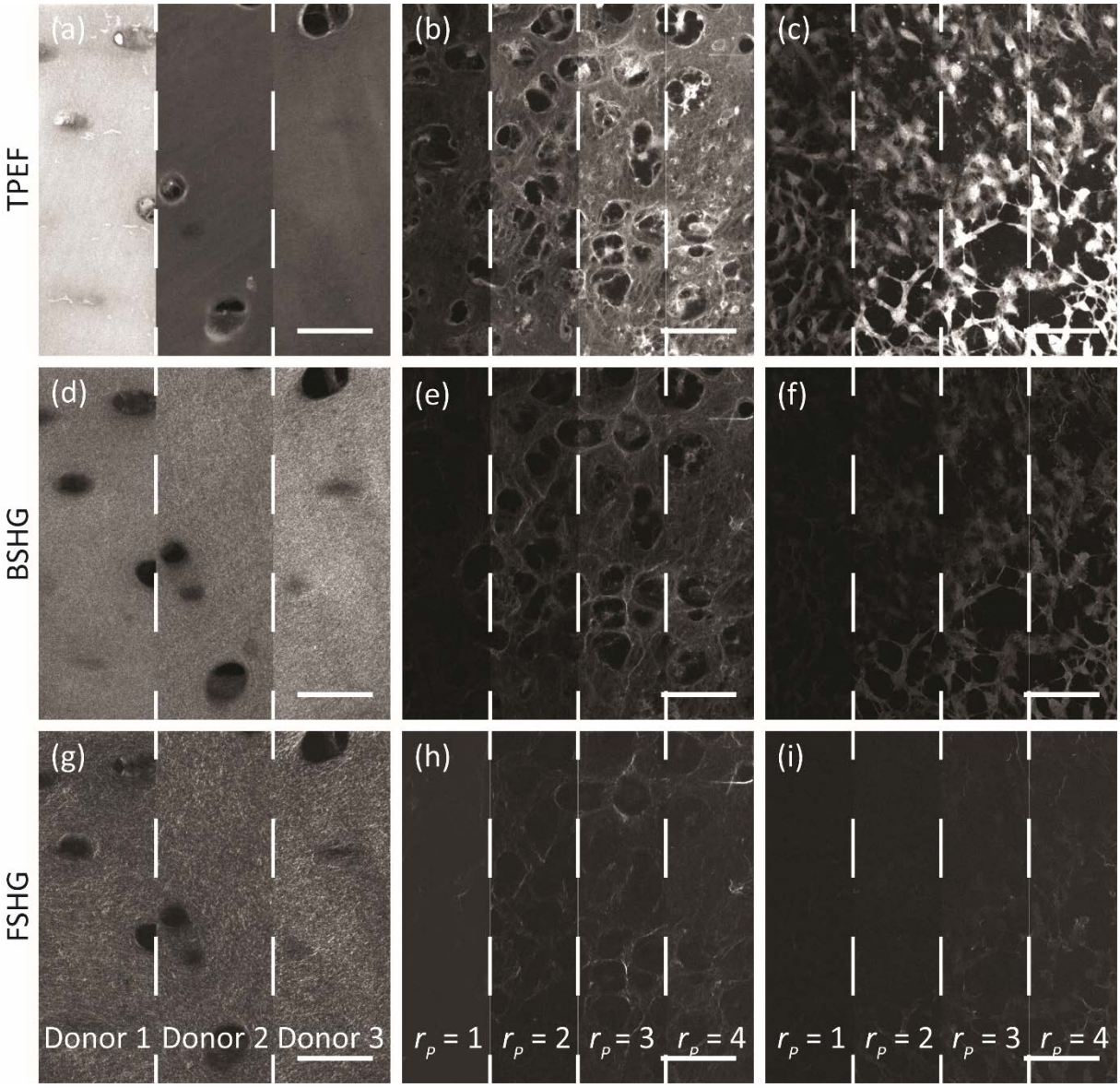

Figure 5. Collagen distribution in ECM among different samples as shown by BSHG. (a) Cartilage, (b) HFPSCs spheroid (+GF) and (c) HFPSCs spheroid (-GF) with their corresponding intensity histograms (d, e and f). The images were segmented into background (red) and ECM containing collagen. The percentage of the image that contains collagen is depicted in the histograms. The tissue-engineered cartilage was imaged at r_p=4. Five separate areas from each of the three cartilage donors were used as a reference sample. The same area as depicted in (b) and (c) were imaged and analysed as dictated by each reference sample. The average determined area with standard deviation was calculated for all reference samples (g), as well as the results based on the five references from each individual donor (h). Scale bar: 50 µm.

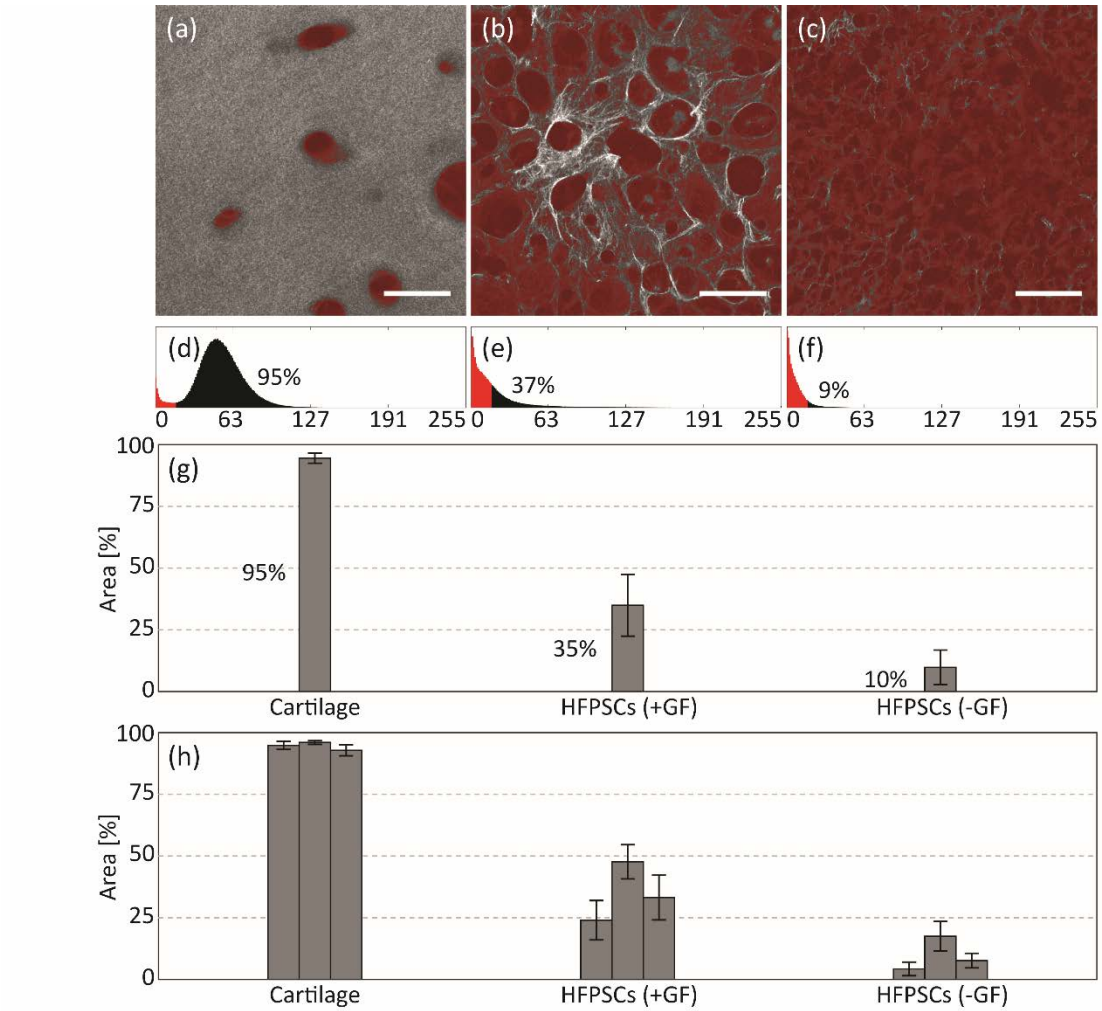

Figure 6. Changes in F/B-ratio in different samples. (a) Cartilage from three different donors, (c) HFPSCs spheroids (+GF) and (e) HFPSCs spheroids (+GF) (green: BSHG, blue: FSHG) with their corresponding F/B ratio (b, d and f). Scale bar: 50 µm.